A splitting scheme for highly dissipative Smoothed Dissipative Particle Dynamics

Sergey Litvinov, [a] Marco Ellero, [a,b] Xiangyu Hu [a]

Nikolaus Adams [a]

[a] *Lehrstuhl für Aerodynamik, Technische Universität München*

85748 Garching, Germany

[b] *Departamento de Física Fundamental, UNED,*

Apartado 60141, 28080 Madrid, Spain

Abstract

Smoothed Dissipative Particle Dynamics (SDPD) is a novel coarse-grained mesoscopic method for the simulation of complex fluids representing the effect of microscopic scales by a stochastic process. It has some advantages over more traditional particle-based methods but, on the other hand, shares some problems common to particle-based simulations of microfluidic systems. In particular a prohibitive stability constraint prevents its application for Schmidt numbers of $O(10^3)$ which is typical for liquids.

In the present paper we propose an implicit numerical scheme for SDPD that allows to increase significantly the time-step size, and thus to perform simulations at significantly larger Schmidt numbers than was possible previously. Simulations using the new method show close agreement with reference scheme results for Couette and Poiseuille flow. Benchmark results for temperature control (i.e. recovery of macroscopic temperature) are also presented. The radial distribution function of

the mesoscopic model liquid is found to be in agreement with experimental results.

1 Introduction

Smoothed Dissipative Particle Dynamics (SDPD) [1], has been introduced as a generalization of the Smoothed Particle Hydrodynamics method (SPH) [2] for describing mesoscopic fluid flows. It is a modification of Dissipative Particle Dynamics (DPD), another popular mesoscopic particle-based scheme [3], consistent with the macroscopic flow. SDPD has the following specific features:

- the method is based on a formally second-order in space discretization of the Navier-Stokes equations;
- transport coefficients can be stated as input parameters and are not an indirect result of other parameters as in DPD;
- hydrodynamic behavior is obtained at length scales of the same order as the particle dimension and no further coarse-graining assumption is required;
- it produces the correct scaling of thermal fluctuations depending on the fluid particle size.

However, despite the favorable properties mentioned above, SDPD shares some disadvantages with DPD. In the present paper we address one of these issues, namely the so-called *Schmidt number problem.*

The Schmidt number is defined as the ratio of momentum diffusivity (viscosity) and mass diffusivity.

$$\mathrm{Sc} = \frac{\mu}{D\rho} \tag{1}$$

where μ is the dynamic viscosity and D is the molecular diffusion coefficient of a specific liquid. In [4] it has been pointed out that, in order to achieve a

realistic liquid behavior, it is essential to realize Schmidt numbers Sc of $O(10^3)$ in the simulations. However, for DPD simulations the typically achieved Sc is much smaller, reproducing conditions similar to that for gases rather than for fluids, i.e. Sc $\sim O(1)$.

Peters [5] suggested that the self-diffusion coefficient D appearing in the definition of the Schmidt number is a molecular diffusivity and therefore it is an ill-defined quantity for coarse-grained systems. Accordingly, one would not need to achieve realistically large Sc, but those conventionally obtained in DPD may be sufficient to capture the hydrodynamic interactions correctly. For example, Jiang et al. [6] found for the DPD simulation of polymer solutions that already at low Schmidt numbers hydrodynamic interactions are recovered and the correct polymer dynamics is obtained. Also SDPD simulations of a polymer molecule suspended in Newtonian solvent with Sc $\sim O(1)$ produced the correct static/dynamic scaling laws in agreement with the Zimm theory [7]. However in contrast with the previous findings, Symeonidis et al. [8,9] it was observed that the agreement between simulation and experiments with respect to the description of non-equilibrium properties of a DNA molecule undergoing a shear flow improves when Sc approaches values for a liquid. Furthermore, Vázquez et al. [10] show results for the diffusion properties of a colloid/polymer for decreasing solvent Schmidt number (i.e. for increasing SDPD fluid-particle resolution), suggesting that, to some extent, the fluid particle Schmidt number can be regarded as a measure for numerical convergence. The physical interpretation of the solvent Schmidt number, however, is not the focus of the current work. It is generally accepted that a realistic Schmidt number based on the size of a suspended macromolecule/colloid is a well-defined quantity and that its related diffusion time scales are generally much larger than the

momentum diffusion time scales of the solvent liquid. The exact realization of such conditions is important for quantitative comparisons of simulations with realistic experiments.

As in SDPD all transport coefficients are specified a priori, a large Schmidt number results in numerical stiffness: the stability constraints of current integration schemes results in huge overwhelming computational cost for large viscosity. With current integration schemes the physically relevant mass-diffusive time scales cannot be achieved. The objective of this paper is to extend an implicit scheme [11,12], developed previously for DPD and SPH, to SDPD, and allows to increase the time step significantly in comparison with standard velocity-Verlet algorithms. No further assumption or modification of the physical model is required. In section 2 we briefly describe the SDPD method; in section 3 the time step limitations typical for velocity-Verlet and Predictor-Corrector schemes are discussed; in section 4 the new integration scheme is presented; sections 5 and 6 are devoted to numerical examples for macroscopic and microscopic flows.

2 Model

2.1 Mesoscopic flow modeling

The flow of an isothermal Newtonian solvent can be described by the Navier-Stokes equations written in a Lagrangian reference frame

$$\frac{d\rho}{dt} = -\rho\nabla\cdot\mathbf{v}$$
$$\frac{d\mathbf{v}}{dt} = -\frac{1}{\rho}\nabla p + \frac{\eta}{\rho}\nabla^2\mathbf{v} \tag{2}$$

where ρ is the material density, $\mathbf{v}$ is the velocity, p is the pressure and η is the dynamic viscosity. An SPH discretization of the Navier-Stokes equations is given by [13]

$$\frac{d\mathbf{r}_i}{dt} = \mathbf{v}_i, \tag{3a}$$

$$\rho_i = m_i \sum_j W_{ij}, \tag{3b}$$

$$\frac{d\mathbf{v}_i}{dt} = -\frac{1}{m_i}\sum_j \left(\frac{p_i}{\sigma_i^2} + \frac{p_j}{\sigma_j^2}\right)\frac{\partial W_{ij}}{\partial r_{ij}}\mathbf{e}_{ij} + \frac{\eta}{m_i}\sum_j \left(\frac{1}{\sigma_i^2} + \frac{1}{\sigma_j^2}\right)\frac{\mathbf{v}_{ij}}{r_{ij}}\frac{\partial W_{ij}}{\partial r_{ij}}. \tag{3c}$$

Here, $\mathbf{r}_i$ and m_i are the position and mass of a particle, respectively, with index i, W_{ij} is a kernel function, σ_i is the inverse of the particle volume, $\mathbf{e}_{ij}$ and r_{ij} are the normalized vector and distance from particle i to particle j, respectively. In order to close these equations, an isothermal equation of state for the pressure is given as

$$p = p_0\left(\frac{\rho}{\rho_0}\right)^\gamma + b, \tag{4}$$

where p_0, ρ_0, b and γ are parameters which may be chosen based on a scale analysis so that the density variation is less than a given value. When a sufficiently stiff equation of state is used (usually $\gamma = 7$), mutual penetration of particles is prevented, and an almost incompressible fluid behavior is reproduced.

Within the SDPD formulation [1,13,14], Eq. (3) represents the deterministic part of the particle dynamics. Using the GENERIC formalism [15,16] thermal fluctuations can be taken into account by postulating the following expressions

for mass and momentum fluctuations

$$d\tilde{m}_i = 0, \tag{5a}$$

$$d\tilde{\mathbf{P}}_i = \sum_j B_{ij} d\overline{\overline{W}}_{ij} \mathbf{e}_{ij}, \tag{5b}$$

where $\overline{\overline{dW}}_{ij}$ is the traceless symmetric part of a tensor of independent increments of a Wiener process, and B_{ij} is defined as

$$B_{ij} = \left[-4k_B T\eta \left(\frac{1}{\sigma_i^2} + \frac{1}{\sigma_j^2} \right) \frac{1}{r_{ij}} \frac{\partial W}{\partial r_{ij}} \right]^{1/2}. \tag{6}$$

Some important properties of this particular set of equations are:

- total mass and momentum are exactly conserved;
- linear momentum is also locally conserved due to the anti-symmetry of the discretization;
- because the model has been developed within the GENERIC framework, it can be shown that the fluid system conserves total energy, and the total entropy is a monotonically increasing function of time [1].

3 Time step limitations

For numerical stability of the velocity-Verlet algorithm, the time-step size is constrained by the following conditions: (1) Courant-Friedrichs-Lewy (CFL) condition

$$\Delta t \leq \Delta t_c = 0.25 \frac{h}{c}, \tag{7}$$

where c is the maximum speed of sound and h is the smoothing length; (2) a time step constraint based on the viscous diffusion

$$\Delta t \leq \Delta t_\mu = 0.125 \frac{h^2}{\mu}. \tag{8}$$

As was noticed by Morris et al. [17], for typical microfluidic simulations characterized by very small Reynolds numbers, condition (8) is dominant. It is therefore desirable to employ a time-integration scheme which relaxes the viscous time-step limit Δt_μ.

One possible approach is to integrate equation (3) by a fully implicit integration scheme. Pagonabarraga et al. [18] found that such a method, employed for DPD, is not very practical due to large computational cost. Monaghan [12] described an implicit integration scheme for handling the interaction between dust and gas particles. The key feature of the method is to treat each pair interaction separately and update their velocities implicitly. The process is iterated by sweeping over all the pairs of interacting particles a certain number of times. More recently, a semi-implicit scheme for DPD was proposed by Shardlow [11], based on replacing the relative velocity at time step n with a semi-implicit velocity. In the work of Nikunen et al. [19] the accuracy and performance of Shardlow's scheme was tested and found to be superior to several other schemes commonly used in DPD.

In this work we present a novel implicit method which can be viewed as a combination of the Shardlow and the Monaghan scheme applied to SDPD. We analyze the performance of the method for conditions which are typical for microfluidic simulations, and in particular we address the previously mentioned Schmidt number problem [9].

4 Semi-implicit integration scheme

In the description of the integration scheme the following notation will be used:

$$d\mathbf{v}_i = \frac{1}{m_i}\left(\mathbf{F}_i^C dt + \mathbf{F}_i^D dt + \mathbf{F}_i^R \sqrt{dt}\right), \tag{9a}$$

$$d\mathbf{r}_i = \mathbf{v}_i dt, \tag{9b}$$

where $\mathbf{F}_i^{\{C,D,R\}} = \sum_j \mathbf{F}_{ij}^{\{C,D,R\}}$ are the resulting conservative, dissipative and random forces acting on particle i expressed as a sum of contributions from all interacting particles. From a mathematical point of view equations (9a) and (9b) represent a system of stochastic differential equations (SDE).

The standard velocity-Verlet scheme is characterized by an explicit calculation of all forces on the right hand side of (9a). Intermediate velocity values are used for the force calculations, which are corrected at the end of each time step (Predictor-Corrector approach). The method gives satisfactory results in many application but the time-step size must satisfy both conditions (8) and (7).

In this paper an alternative time marching scheme is described. The key idea is to split the integration process in such a way that the conservative forces are calculated separately from the dissipative and the random forces. For the conservative terms the common explicit or semi-implicit techniques for SPH can be used. The random and viscous forces (fluctuation-dissipation part) are updated in a pairwise fashion from the particle states at a given time. The structure of the resulting pair interaction is very simple, and it is possible to obtain an implicit method that conserves momentum. In order to develop the new model and clarify its relation to existing implicit methods, in the following

we first give a brief overview of Monaghan's and Shardlow's schemes.

Monaghan's scheme [12]: The method involves a sweep over all pairs of neighboring particles repeated a certain number of times (N_s). Let us consider one specific pair at a given time; the correspondent velocities change according to the following implicit rule (tildes denote new values)

$$\widetilde{\mathbf{v}_i} = \mathbf{v}_i + \frac{1}{2}\frac{1}{m_i}\widetilde{\mathbf{F}_{ij}^D}\frac{\Delta t}{N_s}, \tag{10a}$$

$$\widetilde{\mathbf{v}_j} = \mathbf{v}_j - \frac{1}{2}\frac{1}{m_i}\widetilde{\mathbf{F}_{ij}^D}\frac{\Delta t}{N_s}, \tag{10b}$$

Both particles in the pair are updated simultaneously. Obviously the method conserves linear and angular momentum. Within this loop, for the next considered pair we use the already updated velocity values rather than their values at the beginning of the time step.

In order to increase the accuracy in the case of very high viscosities, besides the backward Euler scheme (10) also a two-stage integration scheme can be used [12]. Note that for $\eta \to \infty$ the resulting velocities at the end of a single pair-step are

$$\widetilde{\mathbf{v}_j} = \widetilde{\mathbf{v}_i} = \frac{m_i\mathbf{v}_i + m_j\mathbf{v}_j}{m_i + m_j}, \tag{11}$$

which is the average initial velocity of the two particles, and follows physical intuition for very viscous flow.

Shardlow's scheme [11]: This scheme applies formal methods from the theory of SDE to the equations of motion in DPD [20]. A Trotter expansion gives a factorized integration scheme similar to that of Monaghan but involving additional random terms in the pair update step. In particular, Shardlow's approach does not use multiple sweeping, instead it describes a first-order (S1) and a second-order splitting (S2) by employing a Strang expansion as

alternative to the first-order Trotter splitting.

Splitting scheme for SDPD: Now we develop the new semi-implicit time-integration scheme. The dissipation term in the SDPD equations (3c) is different from the one used by Monaghan and in the one DPD. Following the arguments of Shardlow, we can write the fluctuation-dissipation terms as

$$d\mathbf{v}_i = \frac{1}{m_i}\mathbf{F}^D_{ij}\frac{dt}{N_s} + \frac{1}{m_i}\mathbf{F}^R_{ij}\frac{dt}{N_s}, \tag{12a}$$

$$d\mathbf{v}_j = -\frac{1}{m_j}\mathbf{F}^D_{ij}\frac{dt}{N_s} - \frac{1}{m_j}\mathbf{F}^R_{ij}\frac{dt}{N_s}, \tag{12b}$$

where N_s is a number of sweeps. This feature of the method we borrowed from Monaghan scheme and found that it considerably decreases overall computational effort especially in case of high viscosity. One possible particle-pair form of the fluctuation-dissipation operator is [11]:

$$\widetilde{\mathbf{v}_i} = \mathbf{v}_i + \frac{1}{2}\frac{1}{m_i}\widetilde{\mathbf{F}^D_{ij}}\frac{\Delta t}{N_s} + \frac{1}{2}\frac{1}{m_i}\mathbf{F}^R_{ij}\frac{\Delta t}{N_s}, \tag{13a}$$

$$\widetilde{\mathbf{v}_j} = \mathbf{v}_j - \frac{1}{2}\frac{1}{m_j}\widetilde{\mathbf{F}^D_{ij}}\frac{\Delta t}{N_s} - \frac{1}{2}\frac{1}{m_j}\mathbf{F}^R_{ij}\frac{\Delta t}{N_s}, \tag{13b}$$

where tilde denotes updated variables at the end of the current sweep. Since $\widetilde{\mathbf{F}^D_{ij}}$ is a linear function of $\widetilde{\mathbf{v}_i}$ and $\widetilde{\mathbf{v}_j}$ equation (13)can be solved explicitly to obtain the updated velocities.

The overall semi-implicit scheme can now be stated:

(I) Perform N_s times sweep over all particle pairs with the following operations:

(a) Explicit part of the velocity update:

$$\mathbf{v}_i \longleftarrow \mathbf{v}_i + \frac{1}{2}\frac{1}{m_i}\mathbf{F}^D_{ij}\frac{\Delta t}{N_s} + \frac{1}{2}\frac{1}{m_i}\mathbf{F}^R_{ij}\frac{\Delta t}{N_s}, \tag{14a}$$

$$\mathbf{v}_j \longleftarrow \mathbf{v}_j - \frac{1}{2}\frac{1}{m_j}\mathbf{F}^D_{ij}\frac{\Delta t}{N_s} - \frac{1}{2}\frac{1}{m_j}\mathbf{F}^R_{ij}\frac{\Delta t}{N_s}, \tag{14b}$$

(b) Implicit part of the velocity update: $\widetilde{\mathbf{F}_{ij}^D}$ being a linear function of the velocity at the next time step, the following equations can be easily solved for the velocity updates:

$$\widetilde{\mathbf{v}_i} = \mathbf{v}_i + \frac{1}{2}\frac{1}{m_i}\widetilde{\mathbf{F}_{ij}^D}\frac{\Delta t}{N_s} + \frac{1}{2}\frac{1}{m_i}\mathbf{F}_{ij}^R\frac{\Delta t}{N_s}, \tag{15a}$$

$$\widetilde{\mathbf{v}_j} = \mathbf{v}_j - \frac{1}{2}\frac{1}{m_j}\widetilde{\mathbf{F}_{ij}^D}\frac{\Delta t}{N_s} - \frac{1}{2}\frac{1}{m_j}\mathbf{F}_{ij}^R\frac{\Delta t}{N_s}, \tag{15b}$$

(II) For all particles update the velocity explicitly by half of conservative force (first part of velocity-Verlet scheme):

$$\mathbf{v}_i \longleftarrow \mathbf{v}_i + \frac{1}{2}\frac{1}{m}\mathbf{F}_i^C\Delta t. \tag{16}$$

(III) For all particles update the positions explicitly:

$$\mathbf{r}_i \longleftarrow \mathbf{r}_i + \mathbf{v}_i\Delta t. \tag{17}$$

(IV) For all particles calculate conservative force:

$$\mathbf{F}_i^C(r_{ij}) \tag{18}$$

(V) For all particles update the velocities explicitly with half of the conservative force (second part of velocity-Verlet scheme):roviderp-down mesoscopic simulations.Opera

$$\mathbf{v}_i \longleftarrow \mathbf{v}_i + \frac{1}{2}\frac{1}{m}\mathbf{F}_i^C\Delta t. \tag{19}$$

(VI) Proceed to the next time step.

Following the arguments of Shardlow [11] we can conclude that the method is first-order accurate in time. Higher-order methods can be obtained by using S2-schemes analogously to those presented in [11].

From numerical experiments, we have found that the number of sweeps N_s

strongly affects the accuracy of the results. For optimum accuracy we have employ the Adaptive Sweeping Scheme of Whitehouse et. al. [21] which can be summarized as follows: for every time step we perform consecutively $N_s = 2^m$ and $N_s = 2^{m+1}$ sweeps with m increasing until the relative error between the evaluated velocities is less then a specific dimensionless tolerance ε. The last calculated velocity is adopted and at the next time step the index m is decreased by one. We have found that a tolerance $\varepsilon = 5 \times 10^{-3}$ gives a good compromise between computational efficency and accuracy.

The relaxed viscous stability on one hand allows for large time-step sizes, while on the other hand may increase the temporal truncation error. In the following section we show that for typical microfluidic conditions the method gives good overall accuracy for simulations performed without thermal fluctuations, and allows for simulations at very large Sc number when thermal fluctuations are included.

5 Validation of the splitting SDPD scheme

In this section simulations of the Couette and Poiseuille flows are performed in order to validate the scheme described above. We measure the overall accuracy by using an L_1-norm error defined as

$$L_1 = \frac{\sum_{i=1}^{N} \left| U_i^{th} - U_i^{SDPD} \right|}{\sum_{i=1}^{N} \left| U_i^{th} \right|} \tag{20}$$

where U_i^{th} and U_i^{SDPD} are components of the theoretical and the simulated velocity fields evaluated at the particle positions $\mathbf{r}_i$, respectively, and N is the total number of particles.

For the Poiseuille test case we consider a laminar flow between two infinite parallel plates placed at $y = 0$ and $y = L$. The flow is initially at rest and it is suddenly driven by a constant body force F parallel to the x-axis. Following Morris [17] we chose the following simulation parameters $F = 10^{-4}\,\mathrm{m/s^2}$ and $L = 10^{-3}\,\mathrm{m}$. The density and kinematic viscosity are $\rho = 10^3\,\mathrm{kg/m^3}$ and $\mu = 10^{-6}\,\mathrm{m^2/s}$, respectively. The maximum velocity at steady state is

$$V_{max} = \frac{FL^2}{8\mu}, \tag{21}$$

which gives a Reynolds number

$$\mathrm{Re} = \frac{Lv_{max}}{\eta} = 1.25 \times 10^{-2}. \tag{22}$$

According to (21), the speed of sound is chosen in order to keep the Mach number equal to 0.1

$$c = 10V_{max}. \tag{23}$$

A series of simulations is performed for $N_y = 10, 20, 40, 80$ particles spanning the y-direction, using the scheme described in the section 4 with $\varepsilon = 5 \times 10^{-3}$ and a time step $\Delta t = 3.125 \times 10^{-4} = 4\Delta t_\mu$.

In Fig. 1(top) a comparison for velocity profiles at time $t_m = 0.63\,\mathrm{s}$ from the theoretical solution and the SDPD solution are shown. At this time the velocity profile is found to be very close to the steady state solution for $t = \infty$. Fig. 2 (top) and Fig. 3(top) show the behavior of the L_1-error for increasing space and time resolution. At least first-oder convergence is observed.

For the Couette test case we consider a laminar flow between two infinite parallel plates, one of which is moving at constant speed. We locate the moving plate at $y = L$ and denote the constant velocity as V_0.

Following Morris [17] we chose the following simulation parameters which are typical for microfluidic systems: $\mu = 10^{-6}\,\mathrm{m}^2/\mathrm{s}$, $V_0 = 1.25 \times 10^{-5}\,\mathrm{m/s}$, $L = 10^{-3}\,\mathrm{m}$ and $\rho = 10^3\,\mathrm{kg/m}^3$. The corresponding Reynolds number is, as in the previous case,

$$\mathrm{Re} = \frac{V_0 L}{\mu} = 1.25 \times 10^{-2}. \tag{24}$$

We chose the speed of sound, again, ten times larger than V_0

$$c = 1.25 \times 10^{-4}\,\mathrm{m/s}, \tag{25}$$

and perform simulations for the same resolution as for the Poiseuille flow. A specific time instant $t_m = 0.16\,\mathrm{s}$ is considered where the SDPD solution and the analytical solution are compared. Fig. 1(bottom) shows the two velocity profiles while in Fig. 2 (bottom) and 3 (bottom) the L_1-norm (20) is plotted at the given time for increasing space and time resolution. Again, first-order convergence of the results is obtained.

[Fig. 1 about here.]

[Fig. 2 about here.]

[Fig. 3 about here.]

The temperature control is an important test of the method. We expect time-averages of the measured kinetic temperature to converge to the input temperature. We take $k_BT = 1\,\mathrm{kg{\cdot}m^2/s^2}$, box size $L = 1.25\,\mathrm{m}$, mass density $\rho = 1\,\mathrm{kg/m^3}$, number of particles $N = 15 \times 15 \times 15 = 3375$, which give the input average thermal velocity of the particles is $v^i_{kin} = \sqrt{3k_BT/m}$ (m is mass of one particle). The speed of sound used in our simulations is $c = 5v_{kin}$ The time step was limited according to the CFL condition (7), while the number of sweeps $N_s = 4$. We found that the choice $N_s = 1$, besides of inaccurate kinetic temperatures, produces also unphysical collisions between particles (which is also observed in [22] for DPD).

The behavior of the average kinetic temperature $T_{kin} = mv^s_{kin}/3k_B$, where v^s_{kin} is the computed average thermal velocity of the particles, for increasing number of sweeps N_s is shown in the figure 4.

[Fig. 4 about here.]

Convergence of the measured kinetic temperature towards the input value T_{th} is observed for increasing N_s. Fig. 4 shows also that our choice $N_s = 4$ introduces error below 5% which is reasonably small. Another validation test for our scheme is represented by the shape of the radial distribution functions (RDF) of the fluid particles describing the solvent. We find that the RDF is not affected by the implicit treatment of the viscous terms and preserves the shape which is typical for liquids, see fig. 5.

[Fig. 5 about here.]

6 Polymer in shear flow

In this section we study the effect of the Schmidt number on the properties of a polymer chain in equilibrium and in a steady-shear flow. As already described in [7], we use FENE potentials to model the interactions between SDPD particles representing neighboring beads of the polymer molecule

$$U_{FENE} = -\frac{1}{2} k R_0^2 \ln\left(1 - \left(\frac{r}{R_0}\right)^2\right), \tag{26}$$

where r is the instantaneous distance between neighboring beads, R_0 is the maximum spring extension and k is the spring constant. The FENE force is superimposed on the hydrodynamic interactions of each polymer-bead and produces the correct scaling laws for static and dynamic properties according to the Zimm theory, see [7] for more details.

Table 1 summarizes the values of Sc and average gyration radii obtained from the simulations for different values of input viscosities. The first conclusion is that the average size of the polymer at equilibrium is nearly independent of Sc over a variation range of approximately 1000. The data for the shear flow imply that the polymer is affected by the Schmidt number of the solvent, producing deviations in $\left\langle R_g^{\text{flow}} \right\rangle$ on the order of 50% over the same range of Sc . The results are in good agreement with the conclusions of [9].

[Table 1 about here.]

7 Polymer in Poiseuille flow

The simulation of a polymer in Poiseuille flow is set up in a box with dimensions $L_x \times L_y \times L_z$ with $L_y = 4.0$, $L_z = 8.0$, and $L_x = 4.0$ is the distance between the walls (at $y = 0$ and $y = L_y$). The flow is driven by a body force in the direction of the z axis. Periodic boundary conditions are employed in the flow and span-wise directions. The number of particles is $N_x \times N_y \times N_z = 10 \times 10 \times 20$ and 20 of them were connected by FENE spring as a model of the polymer. Following [23] we assume a volume fraction of the polymer $\phi = 0.01$ as a good model for a dilute solution. To illustrate the effect of Schmidt number on the distribution of the polymer beads in the channel we perform two simulations with Schmidt numbers of 4.8 and 43, respectively.

In Figure 6 the span wise distribution of polymer mass is shown. We find that the profile is affected by Schmidt number: for lower Schmidt number the depletion region at the center of the channel is more pronounced; for higher Schmidt number the polymer concentration tends to be higher in the center with smaller off-center peaks. These results are in agreement with that in the recent study of Millan et. al [23].

[Fig. 6 about here.]

8 Concluding remarks

We have developed a semi-implicit splitting scheme for highly dissipative SDPD method which is the combination and modification of the Monaghan's scheme for SPH method and Shardlow's scheme for DPD method. To achieve

higher accuracy, the number of sweeps in the present scheme is adjusted adaptively. Numerical experiments show that the present scheme has a great potential in addressing the issue of relatively large Schmidt number. Unlike traditional velocity-Verlet algorithms for which the simulations result to be impractical for Schmidt number higher than $O(1)$ [24], all the simulations shown here require the same computational CPU time but several orders of magnitude in the Schmidt number of $O(10^5)$ can be gained allowing for realistic computations of diffusive flow problems.

References

[1] P. Español, M. Revenga, Smoothed dissipative particle dynamics, Phys. Rev. E 67 (2) (2003) 26705.

[2] J. J. Monaghan, Smoothed particle hydrodynamics, Rep. Prog. Phys. 68 (8) (2005) 1703–1759.

[3] P. Hoogerbrugge, J. Koelman, Simulating microscopic hydrodynamic phenomena with dissipative particle dynamics, Europhys. Lett. 19 (3) (1992) 155–160.

[4] R. D. Groot, P. B. Warren, Dissipative particle dynamics: Bridging the gap between atomistic and mesoscopic simulation, J. Chem. Phys. 107 (11) (1997) 4423–4435.

[5] E. A. J. F. Peters, Elimination of time step effects in dpd, Europhys. Lett. 66 (3) (2004) 311–317.

[6] W. H. Jiang, J. H. Huang, Y. M. Wang, M. Laradji, Hydrodynamic interaction in polymer solutions simulated with dissipative particle dynamics, J. Chem. Phys. 126 (4) (2007) 44901.

[7] S. Litvinov, M. Ellero, X. Y. Hu, N. A. Adams, Smoothed dissipative particle dynamics model for polymer molecules in suspension, Phys. Rev. E 77 (2008) 066703.

[8] V. Symeonidis, G. E. Karniadakis, B. Caswell, Dissipative particle dynamics simulations of polymer chains: Scaling laws and shearing response compared to DNA experiments, Phys. Rev. Lett. 95 (7) (2005) 76001.

[9] V. Symeonidis, G. Karniadakis, B. Caswell, Schmidt number effects in dissipative particle dynamics simulation of polymers, J. Chem. Phys. 125 (2006) 184902.

[10] A. Vázquez-Quesada, M. Ellero, P. Español, Consistent scaling of thermal fluctuations in smoothed dissipative particle dynamics, J. Chem. Phys. 130 (2009) 034901.

[11] T. Shardlow, Splitting for dissipative particle dynamics, SIAM J. Sci. Comput. 24 (4) (2003) 1267–1282.

[12] J. Monaghan, Implicit SPH drag and dusty gas dynamics, J. Comput. Phys. 138 (2) (1997) 801–820.

[13] X. Y. Hu, N. A. Adams, A multi-phase sph method for macroscopic and mesoscopic flows, J. Comput. Phys. 213 (2) (2006) 844–861.

[14] X. Y. Hu, N. A. Adams, Angular-momentum conservative smoothed particle dynamics for incompressible viscous flows, Phys. Fluids 18 (10) (2006) 101702.

[15] M. Grmela, H. Öttinger, Dynamics and thermodynamics of complex fluids. I. Development of a general formalism, Phys. Rev. E 56 (6) (1997) 6620–6632.

[16] H. Öttinger, M. Grmela, Dynamics and thermodynamics of complex fluids. II. Illustrations of a general formalism, Phys. Rev. E 56 (6) (1997) 6633–6655.

[17] J. P. Morris, P. J. Fox, Y. Zhu, Modeling low reynolds number incompressible flows using sph, J. Comput. Phys. 136 (1) (1997) 214–226.

[18] I. Pagonabarraga, M. Hagen, D. Frenkel, Self-consistent dissipative particle dynamics algorithm, Europhys. Lett. 42 (4) (1998) 377–382.

[19] P. Nikunen, M. Karttunen, I. Vattulainen, How would you integrate the equations of motion in dissipative particle dynamics simulations?, Comput. Phys. Commun. 153 (3) (2003) 407–423.

[20] J. M. V. A. Koelman, Cellular-automaton-based simulation of 2d polymer dynamics, Phys. Rev. Lett. 64 (16) (1990) 1915–1918.

[21] S. Whitehouse, M. Bate, Smoothed particle hydrodynamics with radiative transfer in the flux-limited diffusion approximation, Mon. Not. R. Astron. Soc. 353 (4) (2004) 1078–1094.

[22] F. Thalmann, J. Farago, Trotter derivation of algorithms for brownian and dissipative particle dynamics, J. Chem. Phys. 127 (12) (2007) 124109.

[23] J. A. Millan, M. Laradji, Cross-stream migration of driven polymer solutions in nanoscale channels: A numerical study with generalized dissipative particle dynamics, Macromolecules 42 (3) (2009) 803–810.

[24] V. Symeonidis, G. E. Karniadakis, A family of time-staggered schemes for integrating hybrid dpd models for polymers: Algorithms and applications, J. Comput. Phys. 218 (1) (2006) 82–101.

List of Figures

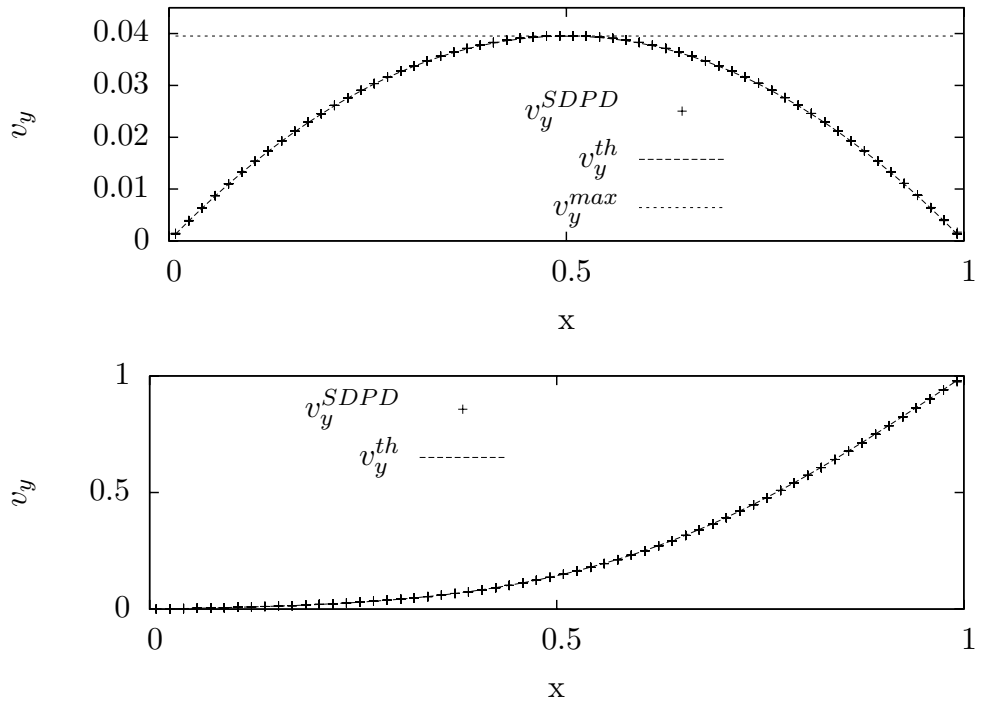

Fig. 1. Comparison of SDPD and theoretical solutions for the Poiseuille flow (top) and the Couette flow (bottom) at time $t_m = 0.63$ and $t_m = 0.16$ respectively ($N_y = 40$).

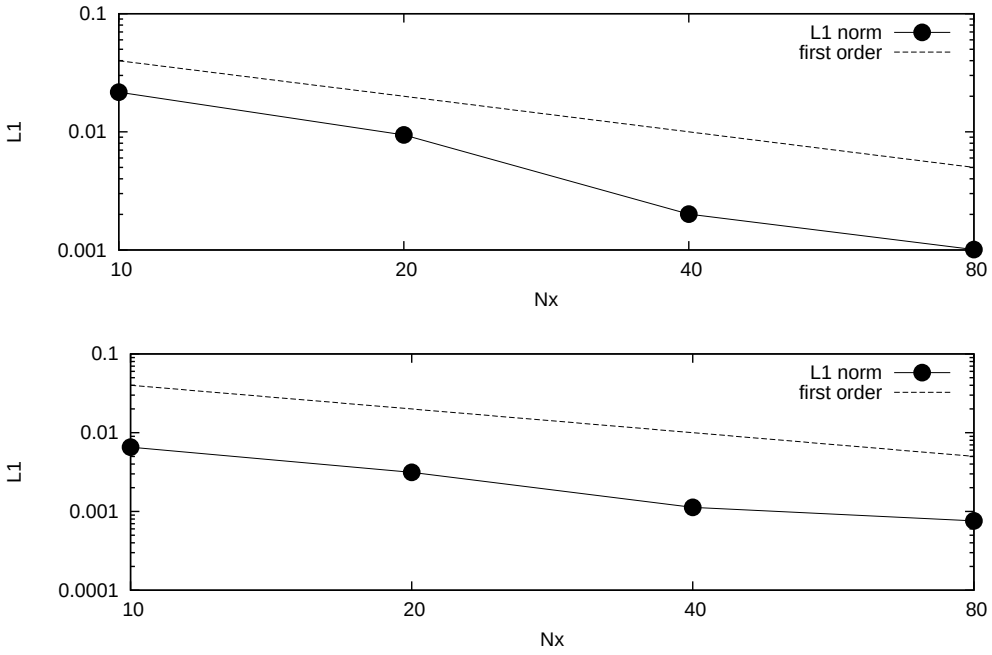

Fig. 2. Comparison of the L_1-norm error for the Poiseuille flow (top) and Couette flow (bottom) as a function of N_y.

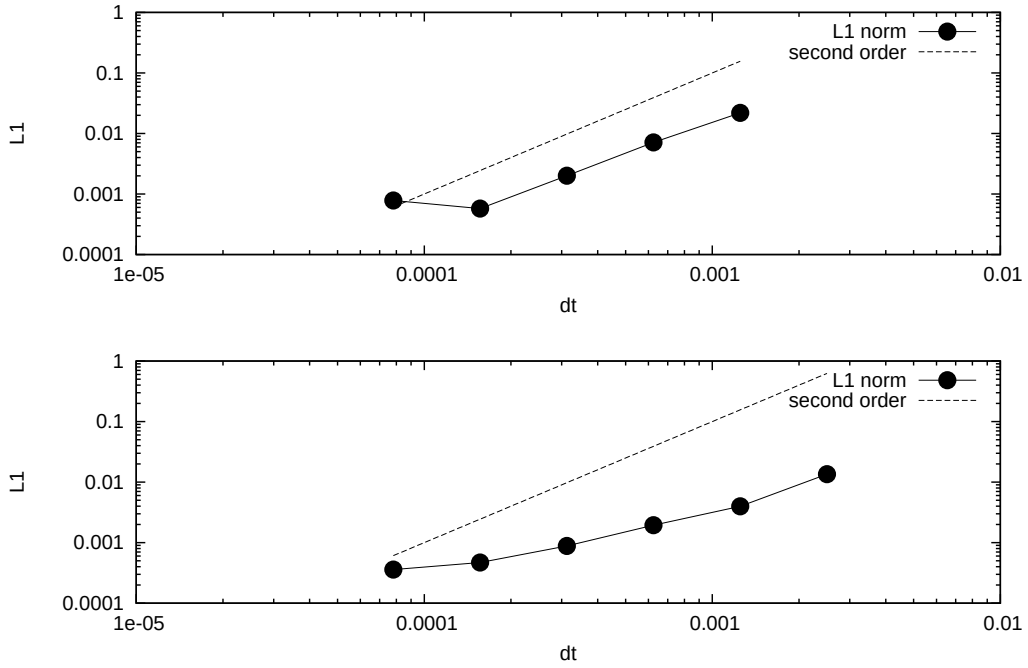

Fig. 3. Comparison of the L_1-norm error for the Poiseuille flow (top) and Couette flow (bottom) as a function of dt.

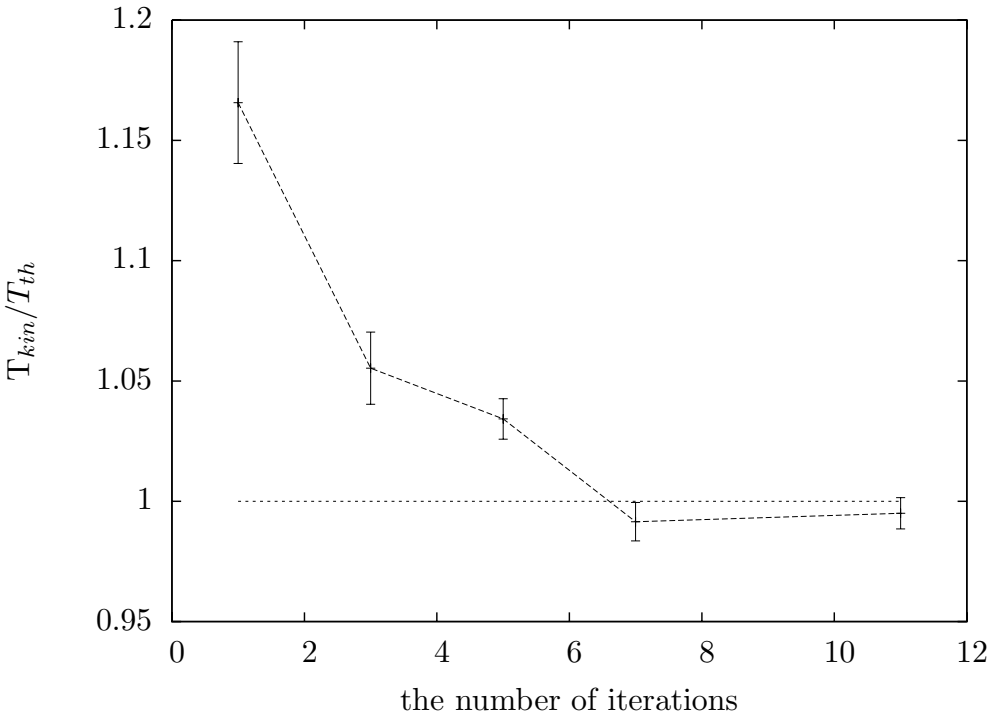

Fig. 4. The measured averaged kinetic temperature for SDPD vs. number of sweeps.

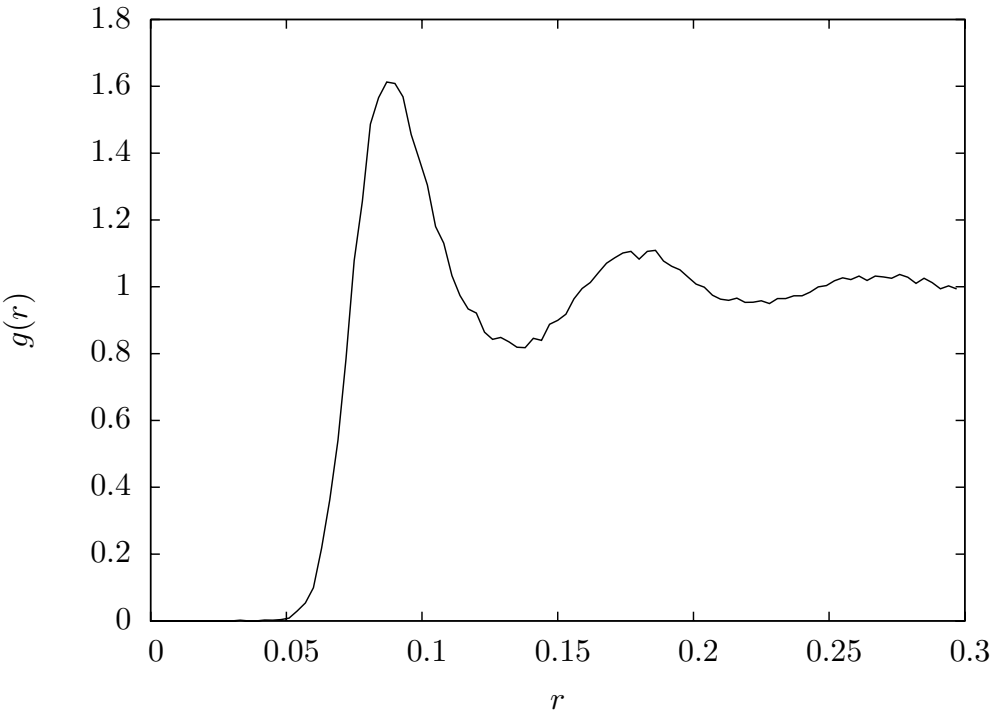

Fig. 5. Radial distribution function for $\mu = 2200.2\,\mathrm{kg/m{\cdot}s}$

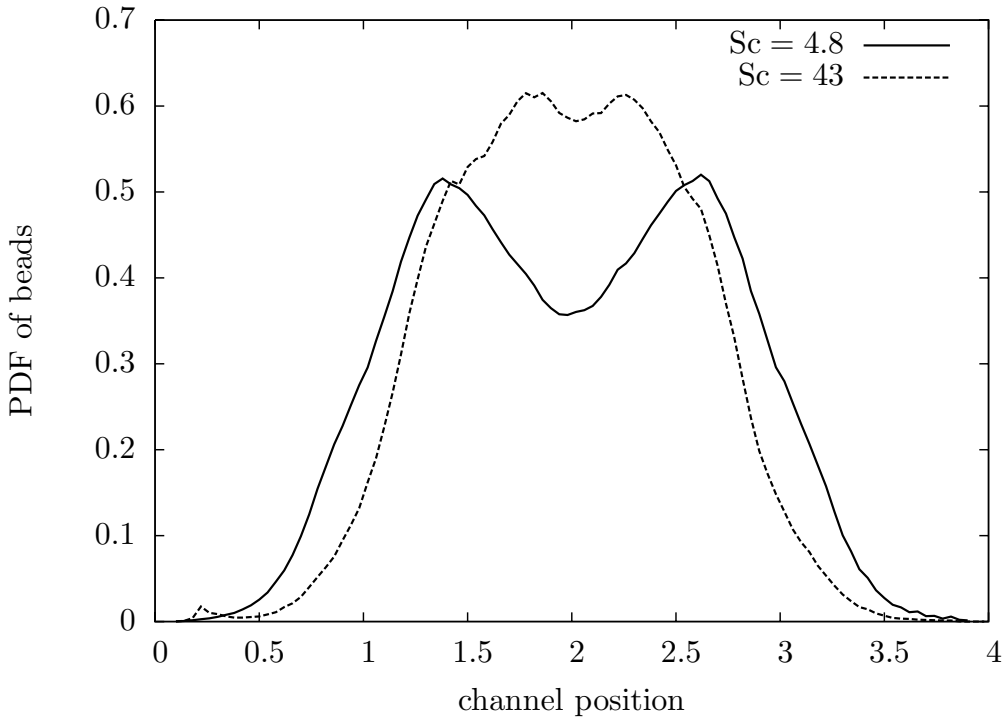

Fig. 6. Polymer bead distribution in Poiseuille flow

List of Tables

Sc	$\langle R_g \rangle$	$\langle R_g^{\text{flow}} \rangle$
1.225e3	0.0048	0.0057
2.5e3	0.0052	0.0058
2.5e5	0.0048	0.0092
1.0e6	0.0048	0.0120

Table 1
Comparison of behavior of free polymer and polymer in a steady shear flow: $k_B T = 1$, $\dot{\gamma} = 0.5$